Exergetic performance analysis of solar air heater with inverted L-shape ribs as roughness element

MANMOHAN CHAUDHARI[a]
SOHAN LAL SHARMA[b*]
AJOY DEBBARMA[b]

[a] Maya Institute of Technology and Management, Selaqui, Dehradun, Uttarakhand-248007, India

[b] National Institute of Technology, Hamirpur, Himachal Pradesh, 177005, India

Abstract Improvement in the exegetic efficiency of a solar air heater (SAH) can be done by enhancing the rate of heat transfer. In this work, the exergetic efficiency optimization of an artificially roughened solar air heater having an inverted L-shape rib has been performed. The numerical analysis of the exergetic performance of the solar air heater was carried out at a constant heat flux of 1000 W/m². The study was conducted to investigate the effect of different relative roughness pitch (7.14–17.86) on the exergy losses, under the Reynolds number range of 3000 to 18 000. The roughness parameter of this geometry has been optimized and found to be among functional operating parameters like average solar intensity and temperature rise across the collector. The optimized value of relative roughness pitch is 17.86 at the isolation of 1000 W/m², and the parameter of temperature rise ranges from 0.005 to 0.04.

Keywords: Solar air heater; Heat transfer; Exergy loss; Exergy efficiency; Thermal efficiency

Nomenclature

A_c – cross-sectional area of the rectangular duct, m²
A_p – area of absorber plate, m²
C_p – specific heat, kJ/kgK

---

*Corresponding Author. Email: sohansh@nith.ac.in

D_h	–	hydraulic diameter of duct, mm
E_x	–	exergy, J
$E_{x\text{loss}}$, El	–	exergy loss, J
e	–	height of L-shape rib, mm
e/D_h	–	relative roughness height
f	–	friction factor
f_s	–	friction factor for smooth duct
h	–	convection coefficient, $\text{W/m}^2\text{K}$
k	–	thermal conductivity of air, W/m K
L, L_2	–	length of test section, mm
L_t	–	total length of the duct, mm
L_1	–	length of inlet section, mm
L_3	–	length of outlet section, mm
$\dot{m}$	–	rate of mass flow, kg/s
Nu	–	Nusselt number
Nu_s	–	Nusselt number for smooth duct
Q_u	–	useful heat gain, W
q, I	–	heat flux applied on absorber surface, W/m^2
P	–	pitch between two successive ribs, mm
P/e	–	relative roughness pitch
ΔP	–	pressure drops, N/m^2
Re	–	Reynolds number
THPF	–	thermohydraulic performance factor of roughened SAH
T_{fi}	–	fluid inlet temperature, K
T_{fo}	–	fluid outlet temperature, K
T_{fm}	–	fluid mean temperature, K
T_{pm}	–	mean absorber temperature, K
ΔT	–	temperature rise of air, K
$\Delta T/I$	–	temperature rise parameter, K/W
El_a	–	exergy loss by the absorber
$\text{El}_{\Delta p}$	–	exergy loss by friction
$\text{El}_{\Delta T}$	–	exergy loss by the air
v	–	velocity, m/s

Greek symbols

η_{exe}	–	exergetic efficiency
η_{eff}	–	effective efficiency
η_{th}	–	thermal efficiency
μ	–	dynamic viscosity of air, kg/m s
ρ	–	density of air, kg/m^3

Subscripts

i	–	inlet
o	–	outlet
fi	–	fluid inlet
fo	–	fluid outlet
u	–	useful

a	–	absorber
s	–	smooth
pm	–	plate mean
fm	–	fluid mean
exe	–	exergetic
eff	–	effective

Acronyms

CFD	–	computational fluid dynamics
HT	–	heat transfer
SAH	–	solar air heater

1 Introduction

It was during the 1973 oil crisis that scientists began looking for ways to balance energy requirements and consumption. 81% of the world's energy needs are met by traditional energy sources like fossil fuels and coal, etc. Traditional fuels and wood burning cause air pollution in agricultural countries. Therefore, it is important to create a heating and cooling system for indoor environments and factories that uses hot air efficiently, sustainably, and cheaply [1, 2]. Because of rising industrialization and population, conventional resources are dwindling and cannot keep up with the rising energy needs of the world. These traditional energy sources are detrimental to humans and have harmed the environment [3, 4]. Although it has been demonstrated that conventional energy sources are limited, monetarily out of reach for many developing nations, and cause environmental damage, the current energy future is heavily weighted toward these sources. The pattern of energy consumption in emerging nations like India predicts a future that is likewise skewed toward the energy that is concentrated in urban centres. A large disparity exists between energy demand and supply because of the lack of access to reliable energy sources in rural regions.

Our natural environment provides a plethora of solar energy that might be harnessed in large quantities. Solar air heaters (SAHs) that use solar energy are common to harness solar energy because of their low cost and ease of use. The SAH is used for a wide variety of heating needs, including crop drying and space heating, etc. The thermal efficiency of SAHs is low in comparison to that of solar water heaters because of the weak heat transfer (HT) capability of air over water. Therefore, increasing the HT coefficient will increase its thermal efficiency. Sharma and Debbarma [5]

reviewed several strategies employed to boost the thermal performance of flat plate SAHs. These techniques mainly include artificial roughness like fins or other geometries. By disrupting the laminar boundary layer, these alterations generate more turbulence and boost heat transmission.

To improve the SAHs' thermal performance several roughness geometries were examined in previous research. Artificially roughened absorber plates enhance the local wall turbulence and create secondary flow. Secondary recirculation flow is responsible for improving the convective HT. Transverse ribs, V-shaped, inclined, W-shaped, and multi-V-shaped ribs are all examples of ribs that may be used to generate turbulence. The height of roughness elements is often maintained at a lower value than the height of ducts. Some characteristics are utilized to determine the geometry and placement of roughness. Prasad and Mullick [6] experimentally examined the impact of protruding wire ribs of circular cross-section on the performance of SAH, used for drying crops. High mass flow rates are employed to generate turbulence in the ducts by introducing protruding wires of 1 mm diameter. The performance of roughened air heaters was enhanced by 14% and increased the HT coefficient from 0.63 to 0.72 using the present wire geometry. Sahu and Bhagoria [7] studied the impact of 900 broken ribs on the thermal performance of a SAH. The fixed roughness height of 1.5 mm and pitch varying from 10 to 30 mm for the range of Re from 3000 to 12 000 were examined. The heat transmission coefficient enhanced from 1.25 to 1.40 times. The roughness pitch of 20 mm yielded the highest Nusselt number (Nu) value, and a thermal efficiency of about 51% to 83.5% was obtained according to the findings. Gupta *et al.* [8] experimentally tested the thermohydraulic performance of a roughened SAH using inclined ribs. The HT and friction factor (f) enhancement for roughened SAH were reported about 1.79 and 2.69 times respectively, for the angle of 70° and 60°. The optimum thermohydraulic performance was recorded for a relative height of roughness 0.023 and Re of 14 000. Karwa *et al.*, [9] conducted experimental research to study the impact of repetitive, 60° inclined rectangular ribs on HT and f for duct aspect ratio varying from 7.19 to 7.75 and Re range from 2800 to 15 000. According to the findings the increase in f about 1.12 to 1.16 times, and enhancement in Stanton number about 22% to 32% were reported as compared to the transverse ribs for 0.0467 to 0.050 relative pitch of roughness. Aharwal *et al.* [10] experimented to study the impact of the width and spacing of square-cross-sectional inclined broken ribs on heat transmission and f. Under the same conditions, the increase in heat transmission for a continuous rib was about 1.48 and 2.26 times, and for

a split rib was about 1.71 and 2.59 times as compared to the smooth duct. For the range of parameters studied, the optimal values of heat transmission, f ratio, and thermohydraulic parameter were found to be associated with a relative gap position of 0.25 and a relative gap width of 1 under Re values 3000 to 18 000. Saini and Saini [11] conducted an experimental study to better understand the impact of the wire mesh absorber on SAH performance under a range of Re varying from 1900 to 3000. The optimum enhancement in the rate of HT was achieved about 4 times concerning the plain duct and the f was claimed to be at its maximum value.

Momin *et al.* [12] tested the effect of V-shaped ribs on the fluid flow and HT properties of the rectangular duct SAH. At 60° attack angle, the result reveals that the Nu and f increase about 2.30 and 2.83 times respectively concerning the plain duct. The Nusselt number was increased by 1.14 and 2.30 times, respectively, when a V-shaped rib pattern was used instead of inclined ribs and a smooth absorber plate. Muluwork *et al.* [13] examined and compared the thermal efficiency of staggering discrete down ribs and V-apex up with equivalent transverse staggered discrete ribs. Effects of various roughness parameters on heat transmission and f were studied including the angle of attack. According to the findings, the maximum heat transmission and f were observed at an attack angle of 60° and 70° respectively. Karwa *et al.* [14] examined heat transmission and f characteristics of SAH using an aspect ratio of 4.8 and 12 and repeated chamfered ribs. The Re range from 3000 to 20 000, the pitch of 4.5 to 8.5, roughness height of 0.014 to 0.0328, and a chamfer angle of 15° to 18° were considered. The Stanton number and the f rose when the chamfer angle was raised and the highest value was achieved at 15° chamfer angle. Bhagoria *et al.* [15] conducted experimental research for SAH using transverse wedge-shaped ribs to analyze the HT and flow properties. Relative roughness height of 0.015 to 0.033 and a rib wedge angle of 80° to 120° were used at the Re range from 3000 to 18 000 for this study. The Nu and f over smooth duct rose by 2.4 and 5.3 times respectively. Saini and Saini [16] looked at how adding arc-shaped ribs to the SAH absorber affected its HT efficiency and frictional resistance. According to the results, the Nu was found to be increased when the relative arc angle decreased, and f decreased with the arc angle. Both Nu and f were observed to increase by a factor of 3.6 and 1.75 respectively at a relative arc angle of 0.3333 and a roughness height of 0.0422 as compared to a plain duct. Saini and Verma [17] examined the impact of dimple-shaped roughened geometry on HT and f. The Re range from 2000 to 12 000 was selected for the investigation. The highest Nu was determined

to correspond to the relative roughness height and pitch of 0.0379 and 10 respectively. At constant relative roughness pitch (i.e., 10) the highest and lowest f were achieved about 0.0289 and 0.0189 respectively. Karmare and Tikekar [18] conducted an experimental investigation for an absorber plate roughened with the grit of metal ribs of a circular cross-section with the goals of heat transmission and friction characteristics enhancement. Nu and f rose by 187%, and 213% with maximum performance at a relative roughness height and pitch of 0.044 and 17.86 respectively.

Hwang and Liou [19] studied the impact of perforated turbulators on the heat transport behaviour of SAH. They examined and compared the thermal efficiency for solid, perforated, and slit turbulence promoters. They employ fences that are either half or perforated, with open area ratios of 0, 10, 22, 38, and 44%. They found that the thermal performance of the permeable fence was superior to the solid-fenced. Sara *et al.* [20] compared the HT from a plate with and without blocks as well as with solid and perforated rectangular blocks, affixed on a flat absorber surface in a SAH. They determined that utilizing perforated blocks might increase energy production by as much as 20%. Increasing the hole diameter, perforation index, and slope of perforated holes can boost HT performance. Sara *et al.* [21] further examined perforated rectangular cross-sectional blocks connected to their surface to enhance heat transmission and found that the rate of heat transmission increased with an increase in the perforation index and that blocks with inclined holes, transfer the heat more efficiently than blocks with straight holes. Greater heat transmission and potential pressure losses are observed with higher f and more compact yields. Buchlin [22] conducted experimental research on the flow through a conduit with perforated ribs at the Re range of 30 000 to 60 000. They conducted experiments with five different Plexiglas rib designs and concluded that a rib pitch ratio of 5 and an open area ratio of 0.53 produce the best results. Moon and Lau [23] performed experimental research with Re varying from 10 000 to 30 000, to investigate heat transmission and pressure drop between two obstructions with the hole in a flow channel. The pressure drop was higher, but the heat transmission was boosted by 4.6–8.1 times due to the obstructions. Though they allow for more heat transmission, smaller holes also result in a greater pressure drop. Karwa *et al.* [24] investigate the impact of perforated baffles integrated into the heated surface on HT and f with Re varying from 2,850 to 11,500. Nu was found to be 60.6 to 62.9, and 45% to 49.7% higher for perforated baffles than for smooth ducts and decreasing with increasing open area ratio from 18.4% to 46.8%, and 73.7% to 82.7% higher for solid

baffles than for smooth ducts. We discovered that the f for solid baffles was 9.6–11.1 times that of a smooth duct, but that it began to fall significantly for perforated baffles as the perforation index increased. Karwa and Maheshwari [25] experimentally investigated the heat transmission and f characteristics of SAH using fully and partially perforated baffles under the Re range of 2700 to 11 150. The perforation index for half and fully perforated baffles were 26% and 46.8%, respectively. The Nu was increased by 79–169% and 133–274% as compared to the smooth duct with fully and half-perforated baffles respectively. On the flip side, the f was found to be 2.98–8.02% higher with fully perforated baffles than with a smooth duct and 4.42–17.56% higher with half perforated baffles. Half-perforated baffles with a relative pitch of 7.2 are found to provide the highest performance about 51.6% to 75.0% as compared to a smooth duct under the same pumping conditions. Liu and Wang [26] did the numerical investigation for semi-attached ribs in SAH under the Re range of 10 000 to 25 000. Results showed that the semi-connected rib design not only outperformed the completely attached and detached rib channels but also considerably improved local HT and fluid flow characteristics. The 45°-angled-rib design with a hole radius to channel width ratio of 0.125 provides the best thermal performance. Nuntadusit *et al.* [27] studied the heat transmission and flow properties of the SAH duct with perforated ribs. They selected the rib hole positions about 0.2H, 0.5H, and 0.8H, and attack angles of 15° and 30° at Re of 60 000. They discovered that angled perforated ribs significantly improved heat transmission in comparison to standard ribs. Ghildyal *et al.* [28] performed a numerical analysis to study the thermo-hydraulic performance of SAH roughened with D-shaped, reverse D-shaped, and U-shaped roughness. Out of the investigated parameters the SAH equipped with U-shaped turbulators exhibited the most favorable thermo-hydraulic performance, achieving the highest factor of 1.76 at a Reynolds number of 4000.

From the foregoing literature study, it can be stated that various investigations have been undertaken on roughened SAHs. However, less research work is done on exergy analysis. The purpose of this study is to analyze the exergetic performance of SAHs having inverted L-shape ribs.

1.1 Novelty and objective of the study

Energy analysis is essential for estimating the performance of the system, while exergy analysis is necessary for investigating how internal irreversibility and systems with varying energy losses actually behave in practice. Ex-

ergy analysis is a crucial method for designing SAHs that make the optimal utilization of the sun's energy. By considering exergy efficiency, researchers may identify the major sources of irreversibility and optimize the system for improved performance.

Therefore, the novelty of this study is to evaluate the exergy efficiency of an SAH with inverted L-shape ribs, which was already examined experimentally and numerically for their thermal efficiency by Gawande *et al.* [29]. This approach provides valuable insights into the system's thermodynamic behaviour, enabling the identification of potential areas for improvement and optimization in terms of energy conversion and overall performance. The comparison plot of exergy efficiency obtained by the proposed model with existing research is shown in Fig. 17 under Section 4 (comparison of the present study with existing research), which shows its novelty over the many previous work.

The primary objective of the present work is to evaluate the exergetic performance of SAH with inverted L-shape ribs as a roughness element by evaluating the various exergy losses. Exergy losses by friction, by the absorber, by working fluid (air), and by convection and radiation are the major losses that are evaluated in this study to analyze the exergy efficiency of the system. The present study has been taken up to explore the effect of relative roughness pitch (P/e), Nusselt number (Nu), friction factor (f), and Reynolds number (Re) on the flow passage as well as on inverted L-shaped ribs. Further subdivisions of the objective are given below:

- to investigate the exergetic losses in inverted L-shaped ribs,

- to determine the effect of these parameters on artificially roughened SAHs,

- to determine the roughness parameter that maximizes exergetic efficiency.

2   Exergy analysis and methodology

The schematic diagrams of the present SAH and the test section with inverted L-shape ribs are shown in Fig. 1a and 1b respectively as explained in existing experimental and numerical studies performed by Gawande *et al.* [29]. The geometry of the SAH duct with three section lengths L_1, L_2 (or L), and L_3 is selected for exergy analysis. By making the duct 20 mm in height and 100 mm in width, the duct has an aspect ratio of 5. The SAH

duct has a hydraulic diameter of $D_h = 33.33$ mm. The top wall of the test portion (L_2) is an aluminium absorber plate. The underside of the duct's top rib is a potential location for an inverted L-shaped rib. The roughness element remains on a plane that is always perpendicular to the flow. Investigated parameters were selected as per the previous research, such as roughness pitch (P/e) varying from 7.14 to 17.86, Re varying from 3000 to 18 000, 1000 W/m^2 heat flux, and constant roughness height (e/D) of 0.042. The geometrical parameters for the inverted L-shape rib considered for the analysis are given in Table 1.
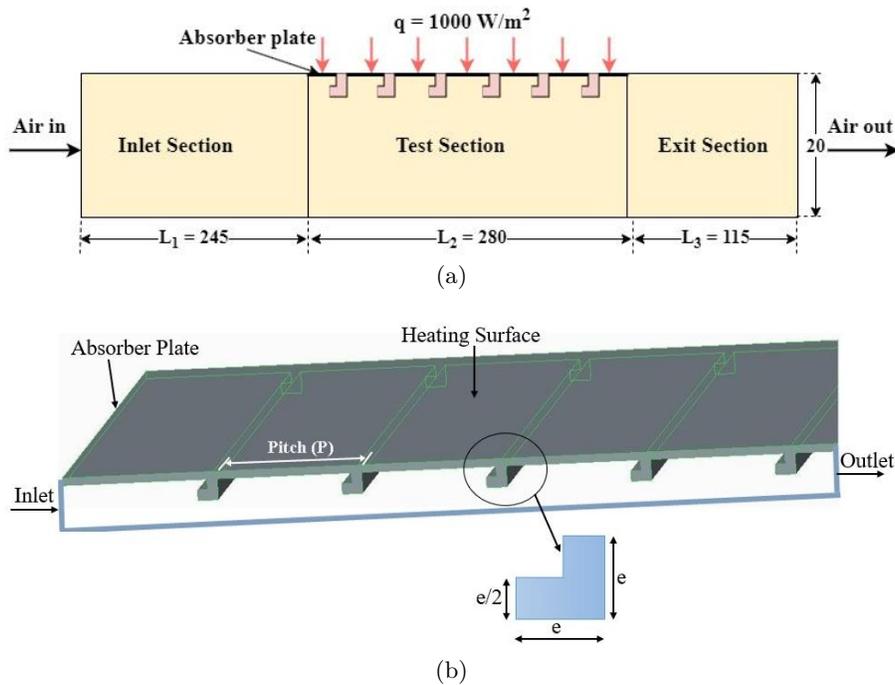

(a)

(b)

Figure 1: Schematic diagram of roughened SAH duct (a), and the test section with inverted L-shape ribs (b).

To evaluate the SAH's efficiency considering the second law of thermodynamics [31,32], it is necessary to analyze the exergy lost and the entropy created in a heat exchanger as a result of heat transfer between two media and friction. Total exergies connected with thermal systems may be expressed mathematically as

$$E_{xT} = {}^{Phy}_T E_x + {}^K_T E_x + {}^P_T E_x + {}^{Ch}_T E_x \,, \tag{1}$$

Table 1: Dimensional details of model and roughness parameters [29].

Roughness and flow parameters	Range of parameters
Hydraulic diameter (D_h)	33.33 mm
Length of inlet section (L_1)	245 mm
Length of test section (L_2)	280 mm
Length of outlet section (L_3)	115 mm
Rib pitch (P)	10 mm, 15 mm, 20 mm, and 25 mm
Rib height (e)	1.4 mm
Relative roughness height (e/D_h)	0.042 (fixed)
Relative roughness pitch (P/e)	7.14, 10.71, 14.29, 17.86

were the physical, kinetic, potential, and chemical constituents of total exergy are denoted as ${}^{Phy}_{T}E_{xT}$, ${}^{K}_{T}E_{x}$, ${}^{P}_{T}E_{x}$, and ${}^{Ch}_{T}E_{x}$, respectively. Under the assumption that all exergy components other than the physical components are insignificant, the balancing equation is expressed as

$$E_{x\mathrm{w}} = E_{x\mathrm{out}} - E_{x\mathrm{in}} + E_{x\mathrm{loss}}, \tag{2}$$

where $E_{x\mathrm{in}}$, $E_{x\mathrm{out}}$ and $E_{x\mathrm{loss}}$ represent the entrance, outflow and loss in exergy:

$$E_{x\mathrm{in}} = \dot{m}\left[(h_{\mathrm{in}} - h_o) - T_o(S_{\mathrm{in}} - S_o)\right], \tag{3}$$

$$E_{x\mathrm{out}} = \dot{m}\left[(h_{\mathrm{out}} - h_o) - T_o(S_{\mathrm{out}} - S_o)\right], \tag{4}$$

$$E_{x\mathrm{loss}} = T_o S_{\mathrm{gen}}. \tag{5}$$

In exergy calculation a dead state condition is required. In equation 5, the term T_o is the dead state temperature (300 K) which is required to calculate the exergy losses, and reference point '0' represent the dead state. At entry, outflow, and reference point, the enthalpy and entropy are all expressed by: h_{in}, S_{in}, h_{out}, S_{out}, and h_o, S_o respectively, $\dot{m}$ is the mass flow rate of air, S_{gen} and T_o represent the entropy generation and reference temperature at dead state.

The exergetic efficiency (η_{exe}) and the energy loss (e) are calculated as follows [33]:

$$\eta_{\mathrm{exe}} = \frac{E_{x\mathrm{out}} - E_{x\mathrm{in}}}{E_{x\mathrm{out}} - E_{x\mathrm{in}} + E_{x\mathrm{loss}}}, \tag{6}$$

$$\mathrm{El} = \frac{E_{x\mathrm{loss}}}{\dot{m}(E_{x\mathrm{in}} - E_{x\mathrm{out}})}. \tag{7}$$

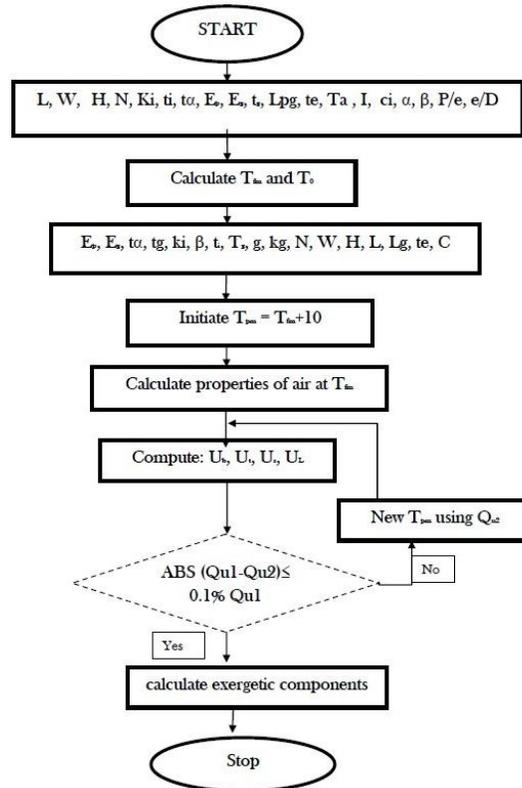The exergy analysis flow chart is shown in Fig. 2.

Figure 2: Flow chart for exergy analysis.

All the parameters are assumed to be noticed at steady state conditions and with the help of these parameters we can calculate the Nusselt number (Nu) and friction factor (f). To calculate the rate of mass flow ($\dot{m}$), useful heat gain (Q_u) by the air to raise their temperature T_{fi} to T_{fo}, and the convection coefficient (h) between air and heated plate, the following equations are used:

$$\dot{m} = C_d A_o \sqrt{\frac{2\rho_w \Delta P_o}{(1 - \beta^4)}}\,, \tag{8}$$

where the orifice plate calibration using a Pitot tube gave a coefficient of discharge (C_d) value equal to 0.608, the pressure drops across the orifice ($\Delta P_o = 9.81\rho_w$) was calculated by a U-tube manometer, ρ_w is the density of

the manometric fluid, A_0 is the area of orifice plate, and $\beta = \dfrac{D_o}{D_p}$ is defined as the ratio of orifice diameter (D_o) and the blower pipe diameter (D_p).

$$Q_{\mathrm{u}} = \dot{m} C_p \left(T_{\mathrm{fo}} - T_{\mathrm{fi}}\right), \tag{9}$$

where C_p is the specific heat capacity of air at constant pressure of 101325 Pa, T_{fi} and T_{fo} represent the temperature of working fluid (air) at the inlet and outlet, respectively, and

$$h = \dfrac{Q_{\mathrm{u}}}{A_p \left(T_{\mathrm{pm}} - T_{\mathrm{fm}}\right)}, \tag{10}$$

where A_p is the area of the absorber surface used to transfer the heat to the air, $T_{\mathrm{fm}} = \dfrac{T_{\mathrm{fi}} + T_{\mathrm{fo}}}{2}$ is the mean temperature of flowing air and T_{pm} is plate mean temperature. These equations determined the Nu and the f in both experimental and computational fluid dynamics (CFD) investigations, mathematically expressed as

$$\mathrm{Nu} = \dfrac{h D_h}{k}, \tag{11}$$

$$f = \dfrac{\Delta P D_h}{2 \rho L v^2}, \tag{12}$$

where k is the thermal conductivity of air, $D_h = \dfrac{2WH}{W + H}$ is the hydraulic diameter, H – height, W – width of a rectangular duct, $L = L_2$ – length of test section, and ρ is the density of air. It is necessary to calculate the hydraulic diameter for a non-circular duct for proper results. The Reynolds number formula can be expressed by

$$\mathrm{Re} = \dfrac{\rho D_h v}{\mu}, \tag{13}$$

where v and μ are known as the flow velocity and dynamic viscosity of air.

The optimum performance of roughened SAH is decided by a factor called thermohydraulic performance factor (THPF) and expressed as

$$\mathrm{THPF} = \dfrac{\dfrac{\mathrm{Nu}}{\mathrm{Nu_s}}}{\left(\dfrac{f}{f_{\mathrm{s}}}\right)^{\frac{1}{3}}}. \tag{14}$$

The standard Dittus–Bolter correlation is used to calculate the $\mathrm{Nu_s}$ for smooth ducts in CFD analysis, mathematically expressed as

$$\mathrm{Nu_s} = 0.023\mathrm{Re}^{0.8}\,\mathrm{Pr}^{0.4}\,. \tag{15}$$

Similarly, for CFD analysis, the standard Blasius correlation to calculate the friction factor for smooth ducts is utilised:

$$f_\mathrm{s} = 0.0791\mathrm{Re}^{-0.25}. \tag{16}$$

Here we see the crucial correlation for forecasting thermohydraulic performance, which is necessary for selecting the best possible geometric parameters in each context. The Nu and f are shown to be effectively influenced parameters with changing P/e and Re during evaluation at a fixed value of e/D [29]:

$$\mathrm{Nu} = 0.023\mathrm{Re}^{0.8332}\left(\frac{P}{e}\right)^{0.3479}\exp^{-0.1004\ln\left(\frac{P}{e}\right)^2}, \tag{17}$$

$$f = 0.2805\mathrm{Re}^{-0.2617}\left(\frac{P}{e}\right)^{0.0815}\exp^{-0.0319\ln\left(\frac{P}{e}\right)^2}. \tag{18}$$

2.1 Validation of the proposed model

Comparisons have been made between the Nu obtained from the present study and those from previously conducted experimental study by Gawande *et al.* [29]. For the experimental validation, the input parameters used in the proposed model were carefully matched with the ones employed in the experimental study. These parameters included boundary conditions, material properties, and operating conditions. The predicted Nu from the present study is compared with the corresponding values obtained from the experimental study as shown in Fig. 3. The mean deviation in the results is obtained in the acceptable range of about 5%. By conducting this validation process, we can assess the agreement between the proposed model and the previously performed experimental model.

The proposed numerical model of SAH with inverted L-shape rib roughness for exergetic analysis is validated under the same operating conditions proposed by Chamoli *et al.* [30]. Fig. 4 shows the plot for exergetic efficiency enhancement across the full range of system and operating parameters corresponding to the temperature rise parameter ($\Delta T/I$). The exergetic efficiency obtained from the proposed model has deviated from the previous research by about $\pm 2\%$. This comparison shows the justification of the proposed numerical model for further investigation.
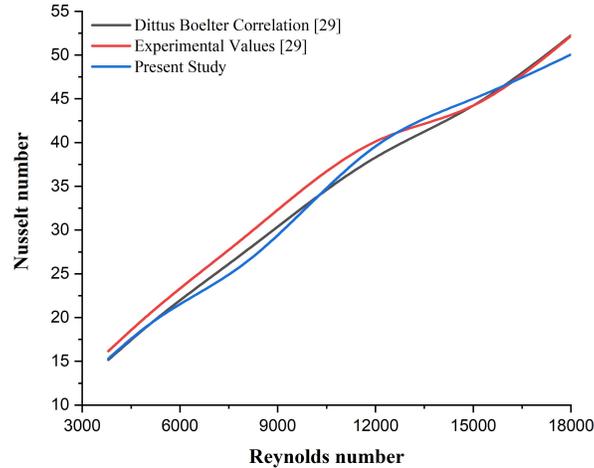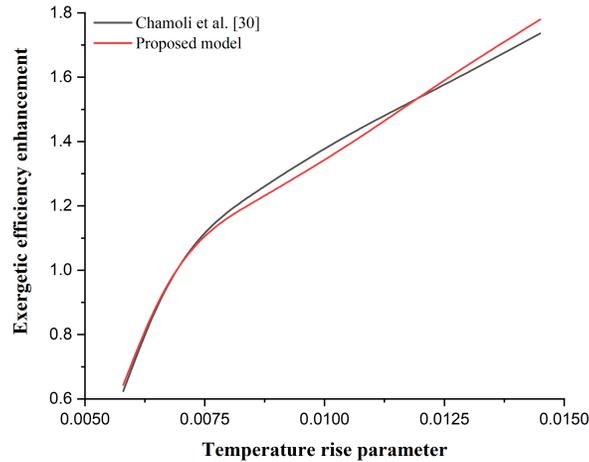
Figure 3: Experimental validation of the proposed model.

Figure 4: Validation of the proposed numerical model with the work of
Chamoli *et al.* [30].

3   Results and discussion

The exergetic performance analysis of SAH having inverted L-shape ribs
has been done at a fixed amount of heat flux, i.e. 1000 W/m^2, variable P/e
(7.14 to 17.86), and Re from 3000 to 18 000. The results obtained from the
exergy analysis are explained as follows:

3.1 Effect of pitch ratio on exergy loss components

3.1.1 Effect of pitch ratio on exergy losses by friction

The conditions that lead to increased friction losses determine the exergy loss. High friction losses and a greater mass flow rate are the results of a lower temperature increase parameter ($\Delta T/I$). Therefore, the lowest possible pitch ratio (P/e) results in the greatest possible exergetic losses. Exertional losses due to friction ($\mathrm{El}_{\Delta p}$) were shown to be positively correlated with the rate of temperature increase shown in Fig. 5.
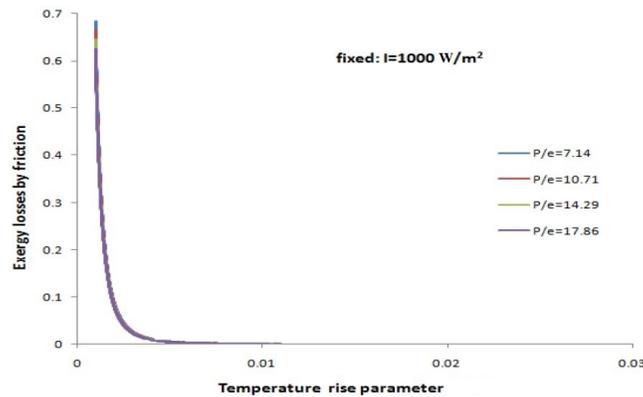
Figure 5: Variation of exergy losses by friction ($\mathrm{El}_{\Delta p}$) with temperature rise parameter ($\Delta T/I$).

3.1.2 Effect of pitch ratio on exergy losses by an absorber

Mean plate temperature (T_{pm}) is used to calculate exergy losses through the absorber (El_{a}). The El_{a} decreases with increasing temperature increase parameter ($\Delta T/I$) as illustrated in Fig. 6. For the simple reason that there is more exergy in the energy present at higher temperatures. Raising the temperature of the absorber reduces the exergy loss through the absorber.

3.1.3 Effect of pitch ratio on exergy losses by working fluid

Exergy losses rise in proportion to the quantity of irreversibility, which grows when the temperature increase parameter is increased. An increase in the temperature increase parameter causes the absorber temperature to rise. That's why the parameter for the temperature increase where the
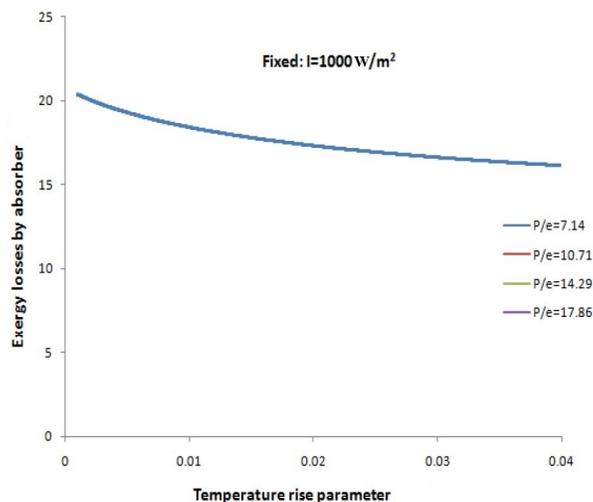
Figure 6: Variation of exergy losses by an absorber (El_a) with temperature
rise parameter ($\Delta T/I$).

exergetic losses by air ($\mathrm{El}_{\Delta T}$) are the greatest is the one with the highest
values. As can be seen in the losses of exergy due to friction increase with
a pitch ratio (P/e) of 7.86, but thereafter they drop and reach a minimum
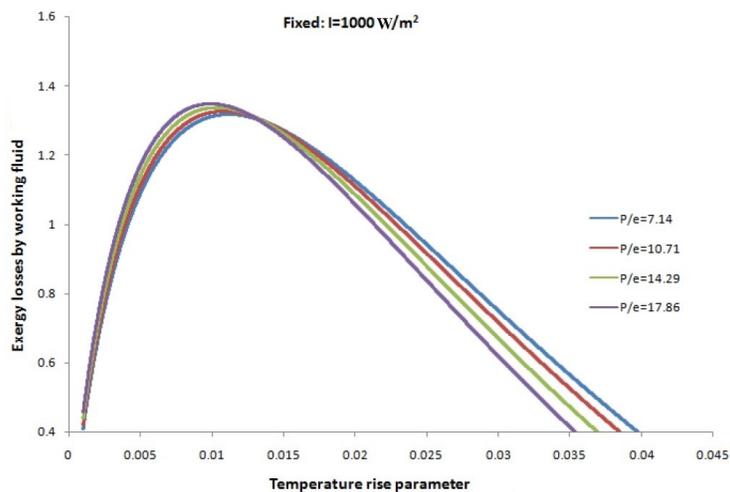for all pitch ratios considered as shown in Fig. 7.

Figure 7: Loss of exergy by air ($\mathrm{El}_{\Delta T}$) corresponds to temperature rise
parameter ($\Delta T/I$).

3.1.4   Effect of pitch ratio on the loss of exergy by convection and radiation

Increasing the temperature increase parameter $(\Delta T/I)$ results in a greater temperature difference between the absorber and surrounding, and hence a greater exergy loss, as shown in Fig. 8. It follows that the smallest temperature increase parameter results in the smallest exergy losses due to heat transmission to the surrounding environment. The exergy loss by the convection and radiation is denoted by El_e, and the values of El_e are highest at pitch ratios (P/e) of 14.29 and lowest at 7.14.
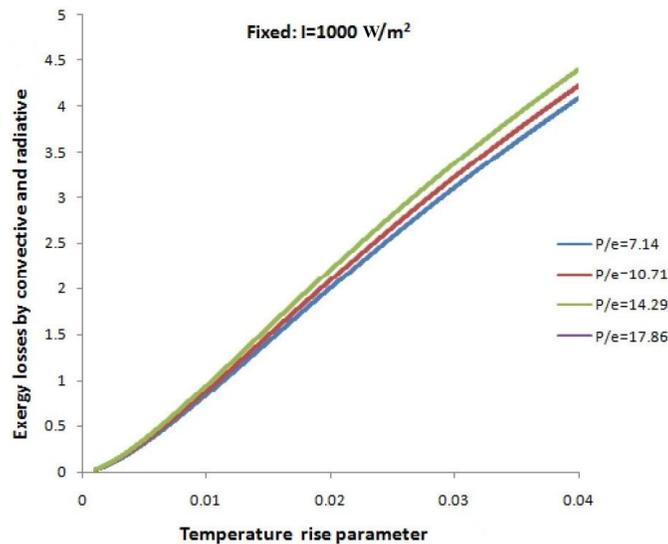
Figure 8: Variation of exergy losses by convection and radiation (El_e) with temperature rise parameter $(\Delta T/I)$.

3.1.5   Effect of pitch ratio on exergetic efficiency

Exergetic efficiency is a function of temperature rise parameter. Exergetic efficiency is negative for low values of the temperature increase parameter $(\Delta T/I)$ due to the extremely high mass flow rate, but it rises as $\Delta T/I$ rise. Exergetic efficiency (η_exe) is illustrated in Fig. 9 for a range of relative pitch (P/e) values, with low values seen for pitch ratios of 17.86 and 7.14, respectively.
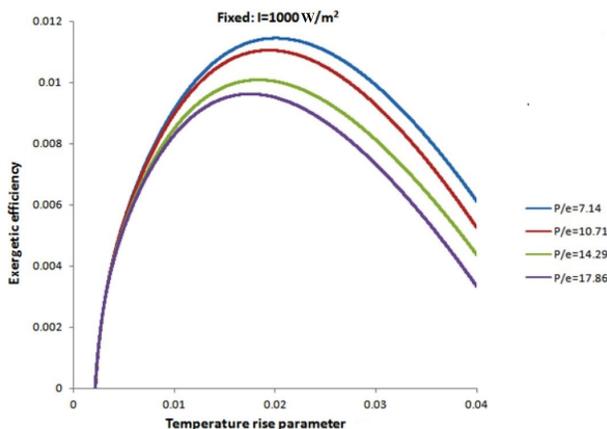
Figure 9: Variation of exergetic efficiency (η_{exe}) with temperature rise parameter ($\Delta T/I$).

3.1.6 Effect of pitch ratio on effective efficiency

Early on, as the Reynolds number rises, effective efficiency improves; it reaches a peak, and then it begins to decline. The domination of mechanical power is what's needed to overcome the forces of friction. The effective efficiency (η_{eff}) drops down dramatically as the temperature increase parameter ($\Delta T/I$) is increased. As can be seen in Fig. 10, it reaches its peak when the temperature rise is rather modest.
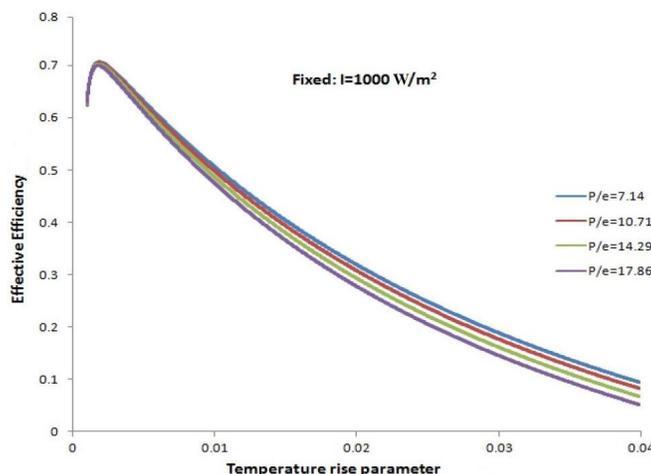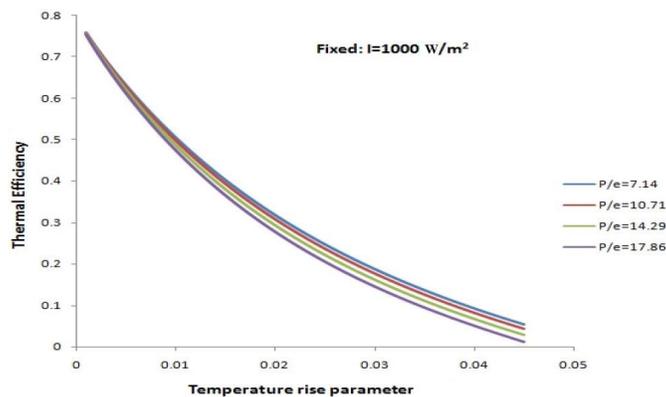

Figure 10: Variation of the effective efficiency (η_{eff}) with temperature rise parameter ($\Delta T/I$).

3.1.7   Effect of pitch ratio on thermal efficiency

When referring to heat transfer, thermal efficiency is measured as the amount of usable heat gained divided by the amount of radiation incident on the absorber. Because of this, it stands to reason that the roughened surface which is accountable for maximizing the usable heat uptake would have the highest thermal efficiency (η_{th}). As the temperature increase parameter ($\Delta T/I$) increases, thermal efficiency deteriorates. When the pitch ratio is at its lowest, $P/e = 7.14$, the thermal efficiency is at its highest as presented in Fig. 11.


Figure 11: Variation of thermal efficiency (η_{th}) with temperature rise parameter ($\Delta T/I$).

3.1.8   Effect of pitch ratio on pressure drop

A significant pressure decrease over the test portion is the price we must pay for optimizing heat transfer. The first law of thermodynamics states that the only allowed change in energy is a change in its form. The turbulence in the test portion is therefore stimulated by a reduction in pressure. As the mass flow rate ($\dot{m}$) increases, the pressure drop (Δp) over the absorber plate does as well, reaching a maximum value for 0.02 kg/s as presented in Fig. 12.

3.1.9   Effect of pitch ratio on the mass flow rate

The mass flow rate is a function of the Reynolds number (Re), and when the value of the Re is increased from 3000 to 18 000, the mass flow rate also rises as shown in Fig. 13.
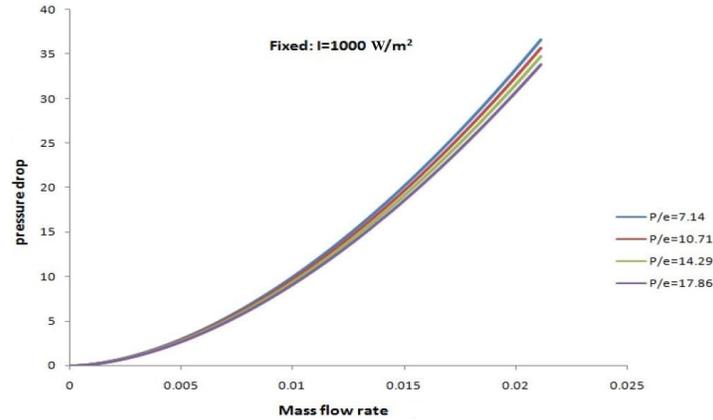
Figure 12: Variation of pressure drop (Δp) with mass flow rate ($\dot{m}$).
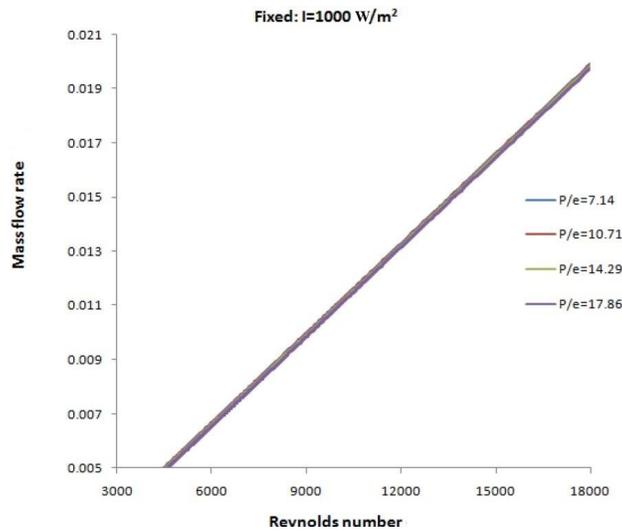
Figure 13: Variation of mass flow rate ($\dot{m}$) with Reynolds number (Re).

3.1.10   Effect of pitch ratio on Nusselt number

In most cases, an increase in the Reynolds number is accompanied by a corresponding rise in the Nusselt number. The value of the Nu concerning the Re attained its maximum for inverted L-shaped roughness at a pitch ratio of 7.14, while concurrently achieving its minimum at a pitch ratio ($P/e = 17.86$) as shown in Fig. 14.
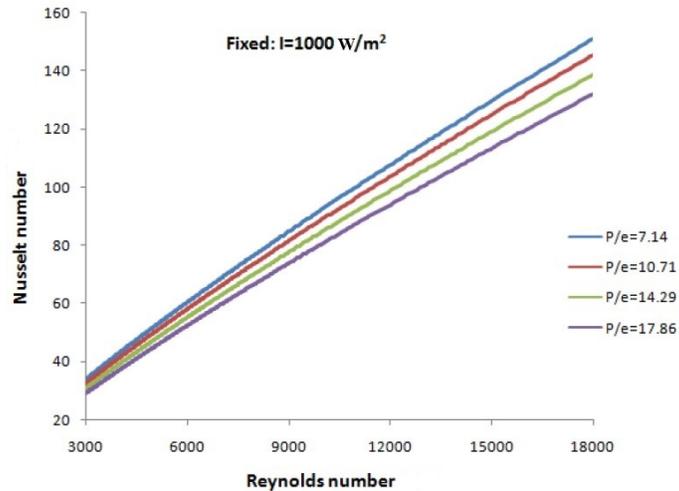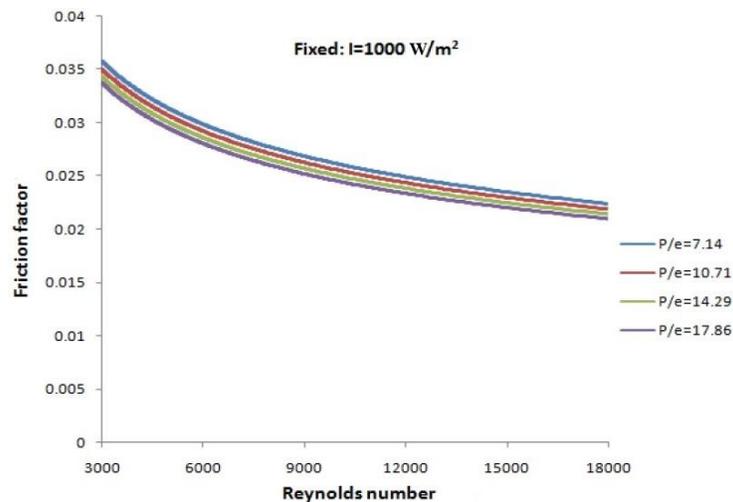
Figure 14: Variation of Nusselt number with Reynolds number.

3.1.11   Effect of pitch ratio on friction factor

The friction factor (f) has a minimum value of $P/e = 17.86$ and a maximum value of $P/e = 7.14$, and its value decreases as the Reynolds number increases as in Fig. 15.

Figure 15: Variation of friction factor (f) with Reynolds number (Re).

3.1.12   Optimization of system parameters

Figure 16 clearly shows that the value of the pitch ratio (P/e) is optimised at an insulation of 1000 W/m^2, and that the value of the temperature rise parameter ($\Delta T/I$) ranges from 0.005 to 0.03, with 17.86 being the optimum value for the relative pitch, as has been shown.
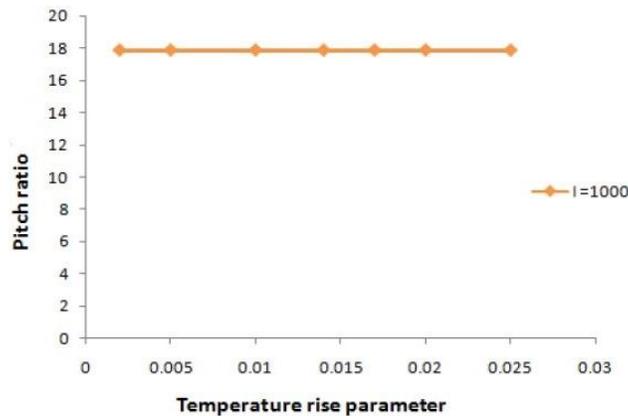

Figure 16: Variation of pitch ratio (P/e) with temperature rise parameter ($\Delta T/I$).

4   Comparison of the present study with existing research

A comparison was made between the results in the literature acquired using different shapes to make it evident how much of an improvement might be made by the proposed numerical model. Exergetic efficiency obtained from the present study is compared to the existing research by Chamoli *et al.* [30]. This comparison of the plot between the present study and previous literature is presented in Fig. 17. Present study offers higher exergetic efficiency at a small temperature rise parameter ($\Delta T/I$) and starts decreasing with a further increase in $\Delta T/I$ when compared to existing literature. After the comparison is concluded that the exergetic efficiency found from the proposed model with an inverted L-shape rib on the absorber plate is larger as compared to the existing work by Chamoli *et al.* [30] at a higher range of $\Delta T/I$, which shows the novelty of the proposed model.
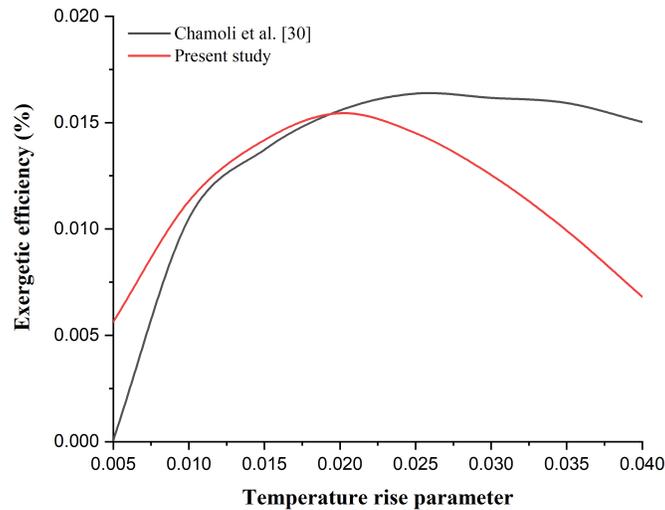
Figure 17: Comparison of the present study with existing research by Chamoli *et al.* [30].

5   Conclusions

In this work, we do a numerical analysis of an inverted L-shape rib on the absorber plate of solar air heater that has been intentionally roughened. Heat transfer improvement and flow friction characteristics as a function of relative roughness pitch and Reynolds number are investigated. Using the exergetic efficiency requirements, the roughness parameters for a given operating state of a SAH were optimized using a Matlab based analytical model.

The following are the study's most significant findings:

- As the Re rises the average value of the Nu increases and the friction factor decreases in general. A fixed value of relative roughness height (e/D_h) and a decrease in relative roughness pitch (P/e) leads to an increase in the average Nusselt number and friction factor.

- At a Re of 15 000, P/e of 7.14, and e/D_h of 0.042, the highest improvement in Nusselt number has been to be about 2.827 times over the smooth duct.

- At P/e of 7.14, the exergetic efficiency of the inverted L-shaped rib is at its highest point, and at P/e of 17.86, it is at its lowest.

- Exergy losses (El) from the absorber plate by convection and radiation heat transfer are the smallest at $P/e = 7.14$ and the largest at $P/e = 14.29$.

- As the temperature increase parameter ($\Delta T/I$) rises, the working fluid's exergy losses from the absorber plate decrease. Exergy losses due to the working fluid are the greatest for $P/e = 17.86$ and the lowest for $P/e = 7.14$.

- As the $\Delta T/I$ increase, the exergy losses *via* absorber (El$_a$) from the absorber plate decrease, and they become nearly equal for all P/e ratios.

- The maximum effective efficiency (η_{eff}) of the inverted L-shaped rib was seen at $P/e = 7.14$ and the minimum efficiency was observed at $P/e = 17.86$, both as a function of the $\Delta T/I$.

- The maximum thermal efficiency (η_{th}) is achieved at $P/e = 7.14$, while the minimal efficiency is achieved at $P/e = 17.86$.

- Gaining a mass flow rate of 0.02 kg/s produces a maximum pressure drop (Δp) from the absorber plate.

The research outcomes of exergy analysis of SAH with inverted L-shape ribs have significant industrial relevance. They provide valuable insights for optimizing system performance, improving energy efficiency, guiding system design and retrofitting, conducting techno-economic assessments, and promoting sustainability in industrial processes.

Received 22 April 2023

References

[1] Singh I., Singh S.: *A review of artificial roughness geometries employed in solar air heaters.* Renew. Sust. Energ. Rev. **92**(2018), 405–425. doi: 10.1016/j.rser.2018. 04.108

[2] Singh I., Singh S.: *CFD analysis of solar air heater duct having square wave profiled transverse ribs as roughness elements.* Sol. Energy **162**(2018), 442–453. doi: 10.1016/ j.solener.2018.01.019

[3] Kalogirou S.A.: *Solar thermal collectors and applications.* Prog. Energ. Combust. Sci. **30**(2004), 3, 231–295. doi: 10.1016/j.pecs.2004.02.001

[4] Omer A.M.: *Energy use and environmental impacts: A general review*. J. Renew. Sustain Ener. **1**(2009), 5, 053101. doi: 10.1063/1.3220701

[5] Sharma S.L., Debbarma A.: *A review on thermal performance and heat transfer augmentation in solar air heater*. Int. J. Sustain. Energ. **41**(2022), 11, 1973–2019. doi: 10.1080/14786451.2022.2125518

[6] Prasad K., Mullick S.C.: *Heat transfer characteristics of a solar air heater used for drying purposes*. Appl. Energ. **13**(1983), 2, 83–93. doi: 10.1016/0306-2619(83)90001-6

[7] Sahu M.M., Bhagoria J.L.: *Augmentation of heat transfer coefficient by using 90 broken transverse ribs on absorber plate of solar air heater*. Renew. Energ. **30**(2005), 13, 2057–2073. doi: 10.1016/j.renene.2004.10.016

[8] Gupta D., Solanki S.C., Saini J.S.: *Thermohydraulic performance of solar air heaters with roughened absorber plates*. Sol. Energ. **61**(1997), 1, 33–42. doi: 10.1016/S0038-092X(97)00005-4

[9] Karwa R.: *Experimental studies of augmented heat transfer and friction in asymmetrically heated rectangular ducts with ribs on the heated wall in transverse, inclined, V-continuous and V-discrete pattern*. Int. Commun. Heat Mass **30**(2003), 2, 241–250. doi: 10.1016/S0735-1933(03)00035-6

[10] Aharwal K.R., Gandhi B.K., Saini J.S.: *Experimental investigation on heat-transfer enhancement due to a gap in an inclined continuous rib arrangement in a rectangular duct of solar air heater*. Renew. Energ. **33**(2008), 4, 585–596. doi: 10.1016/j.renene.2007.03.023

[11] Saini R.P., Saini J.S.: *Heat transfer and friction factor correlations for artificially roughened ducts with expanded metal mesh as roughness element*. Int. J. Heat Mass Tran. **40**(1997), 4, 973–986. doi: 10.1016/0017-9310(96)00019-1

[12] Momin A.M.E., Saini J.S., Solanki S.C.: *Heat transfer and friction in solar air heater duct with V-shaped rib roughness on absorber plate*. Int. J. Heat Mass Tran. **45**(2002), 16, 3383–3396. doi: 10.1016/S0017-9310(02)00046-7

[13] Muluwork K.B.: *Investigations on fluid flow and heat transfer in roughened absorber solar heaters*. Ph.D. thesis, IIT Roorkee, 2000.

[14] Karwa R., Solanki S.C., Saini J.S.: *Heat transfer coefficient and friction factor correlations for the transitional flow regime in rib-roughened rectangular ducts*. Int. J. Heat Mass Tran. **42**(1999), 9, 1597–1615. doi: 10.1016/S0017-9310(98)00252-X

[15] Bhagoria J.L., Saini J.S., Solanki S.C.: *Heat transfer coefficient and friction factor correlations for rectangular solar air heater duct having transverse wedge shaped rib roughness on the absorber plate*. Renew. Energ. **25**(2002), 3, 341–369. doi: 10.1016/S0960-1481(01)00057-X

[16] Saini S.K., Saini R.P.: *Development of correlations for Nusselt number and friction factor for solar air heater with roughened duct having arc-shaped wire as artificial roughness*. Sol. Energy **82**(2008), 12, 1118–1130. doi: 10.1016/j.solener.2008.05.010

[17] Saini R.P., Verma J.: *Heat transfer and friction factor correlations for a duct having dimple-shape artificial roughness for solar air heaters*. Energy **33**(2008), 8, 1277–1287. doi: 10.1016/j.energy.2008.02.017

[18] Karmare S.V., Tikekar A.N.: *Heat transfer and friction factor correlation for artificially roughened duct with metal grit ribs.* Int. J. Heat Mass Tran. **50**(2007), 21–22, 4342–4351. doi: 10.1016/j.ijheatmasstransfer.2007.01.065

[19] Hwang J.J., Liou T.M.: *Heat transfer in a rectangular channel with perforated turbulence promoters using holographic interferometry measurement.* Int. J. Heat Mass Tran. **38**(1995), 17, 3197–3207. doi: 10.1016/0017-9310(95)00065-H

[20] Şara O.N., Pekdemir T., Yapici S., Erşahan H.: *Thermal performance analysis for solid and perforated blocks attached on a flat surface in duct flow.* Energ. Convers. Manage. **41**(2000), 10, 1019–1028. doi: 10.1016/S0196-8904(99)00163-6

[21] Sara O.N., Pekdemir T., Yapici S., Yilmaz M.: *Heat-transfer enhancement in a channel flow with perforated rectangular blocks.* Int. J. Heat Fluid Fl. **22**(2001), 5, 509–518. doi: 10.1016/S0142-727X(01)00117-5

[22] Buchlin J.M.: *Convective heat transfer in a channel with perforated ribs.* Int. J. Therm. Sci. **41**(2002), 4, 332–340. doi: 10.1016/S1290-0729(02)01323-6

[23] Moon S.W., Lau S.C.: *Heat transfer between blockages with holes in a rectangular channel.* J. Heat Transf. **125**(2003), 4, 587–594. doi: 10.1115/1.1576812

[24] Karwa R., Maheshwari B.K., Karwa N.: *Experimental study of heat transfer enhancement in an asymmetrically heated rectangular duct with perforated baffles.* Int. Commun. Heat Mass **32**(2005), 1–2, 275–284. doi: 10.1016/j.icheatmass transfer.2004.10.002

[25] Karwa R. Maheshwari B.K.: *Heat transfer and friction in an asymmetrically heated rectangular duct with half and fully perforated baffles at different pitches.* Int. Commun. Heat Mass **36**(2009), 3, 264–268. doi: 10.1016/j.icheatmass transfer.2008.11.005

[26] Liu H., Wang J.: *Numerical investigation on synthetical performances of fluid flow and heat transfer of semi attached rib-channels.* Int. Commun. Heat Mass **54**(2011), 1–3, 575–583. doi: 10.1016/j.ijheatmasstransfer.2010.09.013

[27] Nuntadusit C., Wae-Hayee M., Bunyajitradulya A., Eiamsa-ard S.: *Thermal visualization on surface with transverse perforated ribs.* Int. Commun. Heat Mass **39**(2012), 5, 634–639. doi: 10.1016/j.icheatmasstransfer.2012.03.001

[28] Ghildyal A., Bisht V.S., Bhandari P., Rawat K.S.: *Effect of D-shaped, reverse D-shaped and U-shaped turbulators in solar air heater on thermo-hydraulic performance.* Arch. Thermodyn. **44**(2023), 2, 3–20. doi: 10.24425/ather.2023.146556

[29] Gawande V.B., Dhoble A.S., Zodpe D.B., Chamoli S.: *Experimental and CFD investigation of convection heat transfer in solar air heater with reverse L-shaped ribs.* Sol. Energy **131**(2016), 275–295. doi: 10.1016/j.solener.2016.02.040

[30] Chamoli S., Thakur N.S.: *Exergetic performance evaluation of solar air heater having V-down perforated baffles on the absorber plate.* J. Therm. Anal. Calorim. **117**(2014), 909–923. doi: 10.1007/s10973-014-3765-8

[31] Kumar S., Kumar R., Goel V., Bhattacharyya S., Issakhov A.: *Exergetic performance estimation for roughened triangular duct used in solar air heaters.* J. Therm. Anal. Calorim. **145**(2021), 3, 1661–1672. doi: 10.1007/s10973-021-10852-w

[32] Yadav S., Kaushal M.: *Exergetic performance evaluation of solar air heater having arc shape oriented protrusions as roughness element.* Sol. Energy **105**(2014), 181–189. doi: 10.1016/j.solener.2014.04.001

[33] Zheng N., Liu P., Shan F., Liu Z., Liu W.: *Heat transfer enhancement in a novel internally grooved tube by generating longitudinal swirl flows with multi-vortexes.* Appl. Therm. Eng. **95**(2016), 25, 421–432. doi: 10.1016/j.applthermaleng.2015.11.066